On crystal-field spectroscopy based on specific heat and thermal expansion measurements: application to the $TmCu_2$ intermetallic compound

1989 J. Phys.: Condens. Matter 1 10153

(http://iopscience.iop.org/0953-8984/1/50/016)

J. Phys.: Condens. Matter **1** (1989) 10153–10163. Printed in the UK

On crystal-field spectroscopy based on specific heat and thermal expansion measurements: application to the $TmCu_2$ intermetallic compound

V Šíma†, M Diviš, P Svoboda, Z Smetana, S Zajac and J Bischof‡
Charles University, Department of Metal Physics, Ke Karlovu 5, 121 16 Prague 2, Czechoslovakia

Received 20 April 1989, in final form 11 July 1989

Abstract. An experimental study based on specific heat, thermal expansion, magnetisation and neutron diffraction measurements on polycrystal and single crystal of the orthorhombic $TmCu_2$ compound is presented. The results are satisfactorily interpreted within a model involving the crystal and molecular field acting on the Tm^{3+} ions. The energy spectrum of the ground-state multiplet $^3H_6$ of Tm^{3+} with the isolated split lowest quasi-doublet ($\Delta_1 = 5 \pm 1$ K, $\Delta_2 = 68 \pm 3$ K) is proposed. The appropriate sets of crystal-field parameters V_l^m are obtained and discussed.

1. Introduction

When the specific heat and thermal expansion of rare-earth compounds are measured, very often a large contribution from the crystal field (CEF) is observed.

We suppose that the Helmholtz free energy F may be expressed as a sum of terms due to the different 'components' of the system, e.g. phonons, conduction electrons and magnetic moments.

Independent additive contributions can then be obtained for the derivatives of F, such as entropy S, specific heat C and bulk modulus B_T, but not for the thermal expansion β, which is a ratio of derivatives, i.e. a ratio of sums. Therefore

$$\beta = [\partial (\ln V)/\partial T]_P$$

$$\beta = -(\partial^2 F/\partial V\, \partial T)/B_T$$

$$B_T = -[\partial P/\partial (\ln V)]_T = V(\partial^2 F/\partial V^2)_T.$$

When we limit our discussion to the low-temperature region, it is not convenient, however, to separate the contributions to the bulk modulus, which is normally dominated by the static lattice energy and varies little with temperature [1]. Hence

$$\beta = \sum_i \beta_i = \frac{1}{B_T} \sum_i \left(\frac{\partial S_i}{\partial V}\right)_T = \kappa_T \sum_i \left(\frac{\partial S_i}{\partial V}\right)_T$$

† Present address: Göttingen University, Institute of Metal Physics, Hospitalstrasse 3-5, 3400 Göttingen, Federal Republic of Germany.

‡ Present address: VÚSE, Běchovice, 190 11 Prague 9, Czechoslovakia.

0953-8984/89/5010153 + 11 $02.50

where the factor κ_T is the isothermal compressibility. The magnitudes of β_i thus depend on the sensitivity of the entropy contribution S_i to the changes in volume.

In this paper we try to describe and exemplify the use of specific heat and thermal expansion data for investigation of the orthorhombic CEF in the $TmCu_2$ compound. Some limitations and possible tests connected with the method are discussed.

$TmCu_2$ is an antiferromagnet below $T_N = 6.3$ K, exhibiting first-order transitions at 4.3 K and near 3 K and a Schottky-type specific heat anomaly between 40 and 50 K [2].

2. Experimental details

Specific heat, thermal expansion and neutron diffraction measurements were performed on a polycrystalline sample; the magnetisation was measured on a single crystal along each principal crystallographic axis.

The polycrystalline sample was prepared by arc melting stoichiometric mixtures of rare-earth metal (purity, 99.9%) and copper (purity, 99.999%) under a protective argon atmosphere; homogenisation annealing was performed in a vacuum quartz tube at 700 °C for 1 week. X-ray diffraction measurements proved the sample to be a single phase. The single crystal of $TmCu_2$ was grown by remelting the polycrystalline material in an alumina crucible under a helium atmosphere and subsequent slow cooling. The specimen (2 mm × 2 mm × 1.5 mm) cut from the bulk was proved to be a single crystal by x-ray analysis. Neutron diffraction measurements on the single crystal revealed several grains with orientations very close to each other. The misorientation of satellite grains is within ±1.5° around the main grain which occupies about 90% of the total volume.

The isobaric specific heat was measured by the quasi-adiabatic method in the temperature range 2.6–82 K; the thermal expansion data were obtained by means of a three-terminal capacitance method from 1.4 to 100 K. The magnetisation measurements were performed on a vibrating-sample magnetometer in magnetic fields up to 5 T and in the temperature range 2–300 K.

3. Results and analysis in the paramagnetic region

In order to analyse the specific heat data above T_N (figure 1) we used the following expression:

$$C = C_e + C_{ph} + C_{Sch}$$

with

$$C_e = \gamma T$$

$$C_{ph} = 27R\left(\frac{T}{\theta_D}\right)^3 \int_0^{\theta_D/T} \frac{x^4 \exp x}{(\exp x - 1)^2}\,dx$$

$$C_{Sch} = \frac{R}{T^2}\left\{\sum_{i=0}^{12} \Delta_i^2 \exp\left(\frac{-\Delta_i}{T}\right) \Big/ \sum_{i=0}^{12} \exp\left(\frac{-\Delta_i}{T}\right) - \left[\sum_{i=0}^{12} \Delta_i \exp\left(\frac{-\Delta_i}{T}\right) \Big/ \sum_{i=0}^{12} \exp\left(\frac{-\Delta_i}{T}\right)\right]^2\right\}$$

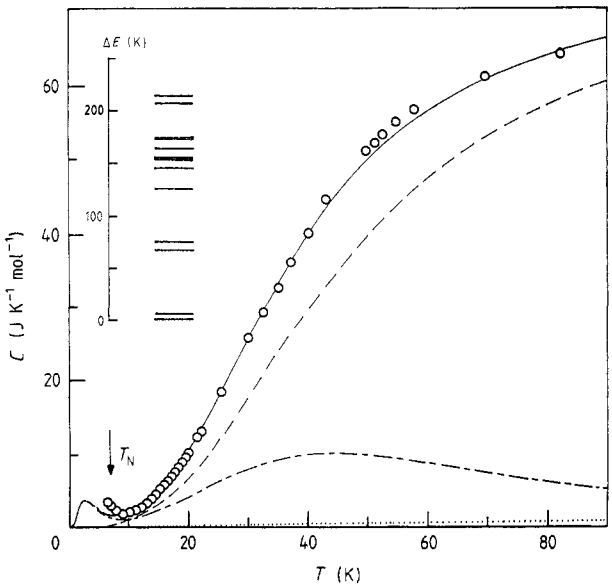

Figure 1. Experimental and calculated temperature dependences of the specific heat of $TmCu_2$ in the paramagnetic region: ○, experimental data; ——, calculated total specific heat; – – –, phonon specific heat; · · · ·, electronic specific heat; — · —, Schottky specific heat. The arrow indicates the Néel temperature. The inset shows the energies of the CEF levels used in calculations.

where C_e and C_{ph} represent the electronic and phonon parts, respectively. C_{Sch} is the Schottky specific heat contribution of Tm^{3+} crystal-field levels. Δ_i is the singlet level energy in kelvins, $i = 0, 1, \ldots, 12$, $\Delta_0 = 0$ K, θ_D is the Debye temperature and R the gas constant.

The electronic contribution to the specific heat in this temperature range is low; we have taken the γ-value equal 9 mJ K^{-2} mol^{-1}, comparable with the values for the other RCu_2 compounds [3]. The phonon part of the specific heat of RCu_2 compounds follows the Debye function rather well, giving for example $\theta_D = 236$ K for YCu_2 and $\theta_D = 198$ K for $GdCu_2$ [3]. From the best fit we obtained $\theta_D = 194 \pm 2$ K for $TmCu_2$.

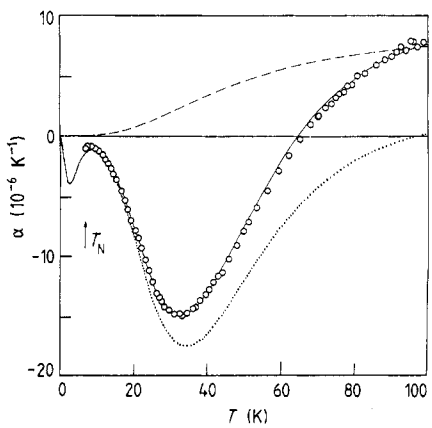

Figure 2. Experimental and calculated temperature dependences of the linear thermal expansion coefficient of $TmCu_2$ in the paramagnetic region: ○, experimental data; ——, calculated total thermal expansion coefficient; – – –, phonon thermal expansion coefficient; · · · ·, Schottky thermal expansion coefficient. The arrow indicates the Néel temperature.

We measured the linear thermal expansion α of an isotropic polycrystalline sample; therefore our analysis is based on the volume thermal expansion $\beta = 3\alpha$ (figure 2). Neglecting the small electronic part of β we can write

$$\beta = \beta_{ph} + \beta_{Sch}$$

with

$$\beta_{ph} = A\gamma_{ph}C_{ph}$$

$$\beta_{Sch} = A\gamma_{Sch}C_{Sch}$$

$$A = \kappa/V$$

$$\gamma_{Sch} = \left\{Z\sum_{i=1}^{12}\Delta_i^2\gamma_i\exp\left(\frac{-\Delta_i}{T}\right) - \sum_{i=1}^{12}\Delta_i\gamma_i\exp\left(\frac{-\Delta_i}{T}\right)\sum_{i=1}^{12}\Delta_i\exp\left(\frac{-\Delta_i}{T}\right)\right\} \Big/ \left\{Z\sum_{i=1}^{12}\Delta_i^2 \times \exp\left(\frac{-\Delta_i}{T}\right) - \left[\sum_{i=1}^{12}\Delta_i\exp\left(\frac{-\Delta_i}{T}\right)\right]^2\right\}$$

$$Z = \sum_{i=0}^{12}\exp\left(\frac{-\Delta_i}{T}\right)$$

$$\gamma_i = -\mathrm{d}(\ln\Delta_i)/\mathrm{d}(\ln V)$$

where the first term represents the phonon part and the second the crystal-field (Schottky) contribution to the thermal expansion, κ is the compressibility, γ_{ph} a lattice Grüneisen parameter, V ($= 31.32 \times 10^{-6}\,\mathrm{m^3\,mol^{-1}}$) the molar volume of $TmCu_2$ and γ_i the crystal-field Grüneisen parameter of the individual energy level Δ_i.

The values of $\kappa(T, V)$ and $\gamma_{ph}(T, V)$ for $TmCu_2$ are unknown as yet. In the case of isostructural YCu_2 and $(Gd, Y)Cu_2$ it was found reasonable that $\kappa\gamma_{ph}$ and θ_D are temperature independent up to 100 K [3]. Similarly for $TmCu_2$ we assume the validity of the approximation that $\kappa\gamma_{ph}$ is independent of temperature and we used a $\kappa\gamma_{ph}$-value of $11.9 \times 10^{-12}\,\mathrm{m^2\,N^{-1}}$, as for YCu_2 [3]. The temperature-independent θ_D indicates that γ_{ph} can also be taken to be temperature independent. Moreover we are able to determine the ratio γ_i/γ_{ph} only and not the individual values of γ_i and γ_{ph} and we have found that the small temperature variation of this ratio does not substantially influence the values of Δ_i.

The problem of interpreting the measured dependences $C(T)$ and $\alpha(T)$ above T_N has been reduced to the determination of parameters θ_D, Δ_i and γ_i. To solve this many-parameter (25) problem, we used a Monte Carlo simulation of all parameters in order to find the intervals of appropriate possible values. The final solution for Δ_i has to conform to the general nine-parameter orthorhombic CEF Hamiltonian, which enables us to reduce the number of parameters to 22 (θ_D, V_l^m, γ_i) and to perform some other physical tests starting from the calculated eigenfunctions of the CEF levels.

The operator of the crystal field acting on rare-earth ions in the $CeCu_2$ structure can be written in the form according to Hutchings [4] as

$$H_{CF} = V_2^0O_2^0(J) + V_2^2O_2^2(J) + V_4^0O_4^0(J) + V_4^2O_4^2(J) + V_4^4O_4^4(J) + V_6^0O_6^0(J) + V_6^2O_6^2(J) + V_6^4O_6^4(J) + V_6^6O_6^6(J).$$

The O_l^m are equivalent operators and V_l^m are the CEF parameters. We treated the latter as adjustable parameters to be determined from the proposed CEF level scheme. The influence of higher multiplets (J mixing) has been neglected in our calculations. The

Table 1. Sets Nos 1–6 are the selected sets of CEF parameters providing the best agreement with specific heat and thermal expansion data. The penultimate row gives the calculated CEF parameters using a simple modification of the PCM (see text); the last row gives the PCM values according to [5]. The table also contains the corresponding value of the calculated saturated moment μ_S.

No	V_2^0 (10^{-23} J/ion)	V_2^2 (10^{-23} J/ion)	(10^{-3}) V_4^0 (10^{-23} J/ion)	(10^{-2}) V_4^2 (10^{-23} J/ion)	(10^{-2}) V_4^4 (10^{-23} J/ion)	(10^{-5}) V_6^0 (10^{-23} J/ion)	(10^{-4}) V_6^2 (10^{-23} J/ion)	(10^{-4}) V_6^4 (10^{-23} J/ion)	(10^{-4}) V_6^6 (10^{-23} J/ion)	μ_S (μ_B)
1	−1.6	−1.1	−2.5	−4.0	3.0	1.0	−9.0	8.0	−11.0	6.39
2	−1.8	−1.2	−0.1	−2.0	0.8	2.0	−13.3	4.0	9.1	6.71
3	−1.8	−1.5	−6.0	−0.6	0.1	2.1	1.0	−16.1	1.2	6.58
4	−1.4	−1.7	0.5	−4.5	3.9	−3.2	−10.4	4.4	6.2	6.25
5	−1.4	−1.7	−0.7	−4.7	5.0	−1.1	−10.3	3.3	4.4	6.21
6	−1.3	−1.8	0.4	−5.1	4.0	−3.5	−10.8	5.6	5.4	6.09
*	−2.0	−0.4	−7.7	−0.5	1.2	4.5	3.4	2.2	−9.9	6.96
$	−1.6	−1.2	0.2	−0.4	1.1	0.6	0.2	0.3	0.3	6.95

omission is permissible because J mixing affects the positions of CEF levels in this case only a little (changes of 0.1 K or less).

Hence we obtained 12 CEF levels above the singlet ground state, which were determined with appropriate experimental errors and nine adjustable CEF parameters V_l^m. The number of possible solutions obeying the experimental conditions is quite large and the numerical procedure strongly depends on the weighting scheme used for the CEF levels. We have previously published one possible solution [5] and the aim of this work is to analyse other sets of V_l^m parameters with respect to experimental data. About 100 fits were done with different numerical weights and starting CEF parameters and the sets of parameters (table 1) which are in agreement with our experimental results have been selected.

The characteristic feature of the CEF splitting of the $^3H_6$ multiplet in $TmCu_2$ is the isolated quasi-doublet ground state with Δ_1 of the order of 1 K ($\Delta_1 = 5$ K; $\Delta_2 = 68$ K) (table 2). This cannot be explained using V_2^0 and V_2^2 only; the higher-order terms (especially V_6^4 and V_6^6) must be taken into account. The specific heat data obtained for the pseudo-binary compound $Tm_{0.2}Y_{0.8}Cu_2$ where the CEF effects are not masked by the magnetic phase transitions down to the limit of the temperature measured (1.5 K) give us a Δ_1-value of 3.5 K.

Starting from the total magnetic entropy of the $^3H_6$ multiplet ($R \ln(2J+1)$) and calculating $\int_{T>T_N}^{\infty}(C_{Sch}/T)\,dT$, we can determine the magnetic entropy $S_m(T)$ above T_N (figure 3) and the absolute entropy scale at low temperatures (see below). The value of $S_m(T)$ for the lowest temperature must be positive, quite close to zero—it acts as an integral test for the determined energy level scheme. The plateau on the $S_m(T)$ curve between 8 and 15 K ($S_m \simeq 5.8$ J K^{-1} mol^{-1}) can be used as another indirect proof of the isolated ground-state quasi-doublet ($R \ln 2 = 5.76$ J K^{-1} mol^{-1}).

All the proposed sets in table 1 were tested by comparison of the calculated saturated magnetic moment μ_S^{calc} in the $\boldsymbol{b}$ direction ($\mu_S^{calc} = g_J\mu_B\langle\Gamma_g|J_z|\Gamma_e\rangle$; $g_J = \frac{7}{6}$) with the measured value $\mu_S^{exp}(6.8 \pm 0.2)\mu_B$ per Tm ion. All sets are in agreement with the anisotropy of the magnetisation in the paramagnetic state, and the ground-state $|\Gamma_g\rangle$ and the first-excited-state $|\Gamma_e\rangle$ eigenfunctions have the postulated Γ_1, Γ_2 symmetry [6].

The values of the molar paramagnetic susceptibility along each crystallographic axis

Table 2. The proposed CEF energy levels and the Grüneisen parameters γ_i/γ_{ph} for Tm^{3+} ions in $TmCu_2$.

i	Δ_i [K]	γ_i/γ_{ph}
0	0	0
1	5 ± 1	−9
2	68 ± 3	−8
3	75 ± 3	−13
4	125 ± 5	−89
5	144 ± 5	−89
6	154 ± 14	−1
7	155 ± 14	0
8	162 ± 12	1
9	171 ± 6	58
10	172 ± 6	44
11	206 ± 12	13
12	214 ± 14	5

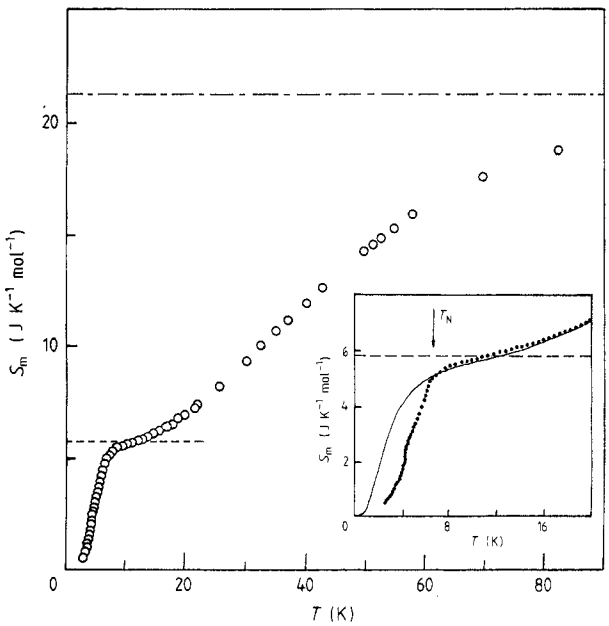

Figure 3. Temperature dependence of the molar magnetic entropy of $TmCu_2$: ○, magnetic part of entropy calculated for experimental specific heat data; ---, $R\ln 2$ for the doublet; — · —, $R\ln(2J+1)$ for the total magnetic entropy. The inset shows the detail of this dependence below 20 K (●) in comparison with calculated magnetic entropy (——) according to the proposed level scheme. The arrow indicates the Néel temperature. Below this temperature can be seen the influence of magnetic phase transitions on the magnetic entropy.

(figure 4) were obtained as M/H from temperature dependence of magnetisation taken in magnetic fields $\mu_0 H = 1$, 2 and 3 T and fitted to the Curie–Weiss law:

$$\chi^i_{\text{mol}} = C^i_{\text{mol}}/(T - \theta_i) \qquad i = a, b, c$$

in order to obtain direct experimental values of V_2^0 and V_2^2.

The fitting procedure gives us the values of the paramagnetic Curie temperatures for each crystallographic direction, $\theta_a = -15$ K, $\theta_b = 49$ K and $\theta_c = 18$ K, and the related effective moments, $\mu^a_{\text{eff}} = (7.1 \pm 0.2)\mu_B$ per Tm ion, $\mu^b_{\text{eff}} = (7.5 \pm 0.2)\mu_B$ per Tm ion and $\mu^c_{\text{eff}} = (7.5 \pm 0.2)\mu_B$ per Tm ion, quite close to the value for a free Tm^{3+} ion ($7.56\mu_B$).

The paramagnetic Curie temperatures can be derived on the basis of the molecular field theory according to [7] as

$$\theta_a = \theta_p + (2J+1)(2J+3)(V_2^0 + V_2^2)/10k_B$$
$$\theta_b = \theta_p - (2J+1)(2J+3)V_2^0/5k_B$$
$$\theta_a = \theta_p + (2J+1)(2J+3)(V_2^0 - V_2^2)/10k_B$$
$$\theta_p = (\theta_a + \theta_b + \theta_c)/3.$$

The second-order CEF parameters $V_2^0 = (-1.3 \pm 0.3) \times 10^{-23}$ J/ion and $V_2^2 = (-1.4 \pm 0.4) \times 10^{-23}$ J/ion were calculated using the experimental θ_a, θ_b and θ_c and also $\theta_p \simeq 17$ K.

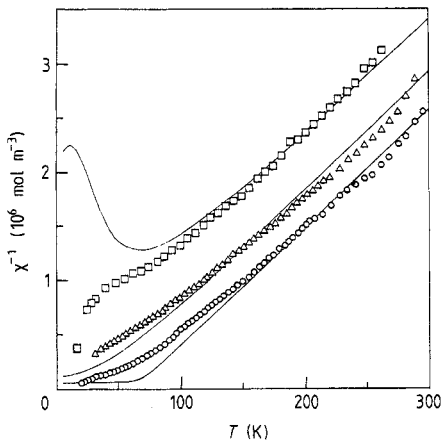

Figure 4. Temperature dependences of the reciprocal magnetic susceptibility of $TmCu_2$ along each principal crystallographic direction: □, experimental data obtained along the ***a*** axis; ○, experimental data obtained along the ***b*** axis; △, experimental data obtained along the ***c*** axis; ——, calculated values according to the set of CEF parameters No 6 (table 1).

The paramagnetic susceptibility was calculated (for magnetic fields $\mu_0 H = 1, 2$ and 3 T) assuming the general single-ion Hamiltonian

$$\mathcal{H} = \mathcal{H}_{CEF} - g_J \mu_B (H + \lambda M) J_z$$

where λ is the molecular-field constant and M is the z component of magnetisation. We have used our proposed sets of V_l^m and the transformation properties of Stewens equivalent operators [4] in order to express the temperature dependence of susceptibility $\chi = M/H$ along the principal crystallographic axes ***a***, ***b*** and ***c*** [7]. The comparison between experimental and calculated susceptibility (using set of V_l^m parameters No 6) can be seen in figure 4.

4. Magnetic ordered state

$TmCu_2$ is an antiferromagnet below $T_N = 6.3$ K. The second-order transition is clearly reflected in the specific heat data [2], in the thermal expansion [8] and magnetisation [9]. The next first-order phase transition occurs at 4.3 K [8, 9]. There are some experimental indications for another first-order transition near $T = 3$ K, which seems to be extremely sensitive to internal stresses [8].

The powder neutron diffraction pattern obtained at 5 K contains two types of magnetic reflection: satellites $(h \pm \frac{1}{3}, k, l)$ where $h + k + l$ is odd and non-satellite magnetic peaks (h, k, l), $h + k + l$ odd. A detailed analysis of the observed pattern revealed that the moment component connected with the first type of reflection is transversally modulated with a propagation vector $\frac{1}{3}\boldsymbol{a}^*$ and moments parallel to the ***b*** direction. The second type of reflection is responsible for a moment component parallel to the ***a*** axis, similar to the component observed in $TbCu_2$ [10]. By analogy, the resulting magnetic structure in $TmCu_2$ is non-collinear and its magnetic moments may be described [10] by

$$\boldsymbol{M}_{1,n} = -\boldsymbol{\alpha} + \boldsymbol{\beta} \cos(\tfrac{1}{3}\boldsymbol{a}^* \cdot \boldsymbol{R}_n)$$

$$\boldsymbol{M}_{2,n} = \boldsymbol{\alpha} + \boldsymbol{\beta} \cos(\tfrac{1}{3}\boldsymbol{a}^* \cdot \boldsymbol{R}_n)$$

$$\boldsymbol{M}_{3,n} = \boldsymbol{\alpha} - \boldsymbol{\beta} \cos(\tfrac{1}{3}\pi + \tfrac{1}{3}\boldsymbol{a}^* \cdot \boldsymbol{R}_n)$$

$$\boldsymbol{M}_{4,n} = -\boldsymbol{\alpha} - \boldsymbol{\beta} \cos(\tfrac{1}{3}\pi + \tfrac{1}{3}\boldsymbol{a}^* \cdot \boldsymbol{R}_n)$$

where $\boldsymbol{R}_n = n_1\boldsymbol{a} + n_2\boldsymbol{b} + n_3\boldsymbol{c}$, n_i are integers, $\boldsymbol{\alpha} \parallel \boldsymbol{a}$ and $\boldsymbol{\beta} \parallel \boldsymbol{b}$, $|\boldsymbol{\alpha}| = (2.8 \pm 0.5)\mu_B$ and $|\boldsymbol{\beta}| = (3.5 \pm 0.5)\mu_B$. This structure has two magnetic moments μ_1 and μ_2 given by $\mu_1 = \sqrt{\alpha^2 + \frac{1}{4}\beta^2}$ and $\mu_2 = \sqrt{\alpha^2 + \beta^2}$. The proposed model was tested by profile analysis of the powder pattern. The reliability factors were about 16% for the nuclear and about 26% for the magnetic structure. In spite of the rather large R-factors we find the model reasonable because the data were collected at a temperature just above the transition temperature (4.3 K). Therefore there may be a mixture of magnetic phases in the powder sample owing to the low thermal conductivity of the powder.

The existence of the $\boldsymbol{b}$ axis component was expected from the anisotropy behaviour of the paramagnetic susceptibility in accordance with the lowest-quasi-doublet wavefunctions with Γ_1, Γ_2 symmetry [6]. However, the existence of the $\boldsymbol{a}$ axis component is difficult to explain from the CEF level scheme ($\mu_a = g_J\mu_B\langle\Gamma_1|J_y|\Gamma_2\rangle = 0$). The perturbation from excited states acting by means of exchange interaction on the ground state is small and cannot explain the observed $\boldsymbol{a}$ axis component of the moment. On the other hand, the calculated magnetisation along the $\boldsymbol{a}$ axis including this contribution of excited states is in good agreement with the observed $\boldsymbol{a}$ axis magnetisation (the $\boldsymbol{a}$ axis is the magnetically hard axis) [9].

However, it can be shown that the appropriate $\pm\alpha$ moments conform to anisotropic properties of the dipole–dipole interaction. This interaction prefers the parallel alignment of two magnetic moments longitudinally oriented to their connecting line and the antiparallel alignment of magnetic moments perpendicularly oriented to their connecting line. In $TmCu_2$ the dipole–dipole energy is approximately of the order of 1 K and therefore it can influence details of the magnetic structure.

5. Discussion

By inspecting table 1, we can make the following conclusions concerning the CEF in $TmCu_2$. The major contribution to the CEF splitting comes from the second-order terms V_2^0 and V_2^2. This is a well known feature of CEF in RCu_2 compounds, because many of the bulk properties can be described in the second-order approximation only. These terms, however, cannot satisfactorily describe the observed splitting of the ground-state quasi-doublet ($\Delta_1 = 5.7$ K) and the inverse susceptibility χ_a^{-1} behaviour between 20 and 70 K. All nine parameters V_l^m must be taken into account in order to obtain at least qualitative agreement with measurements.

One obtained solution (No 1) was previously compared with the point-charge model (PCM) [5]. These calculations confirmed that the second-order parameters are consistent, if the shielding parameter σ_2 is taken to be 0.75 in accordance with other RCu_2 compounds, and close to that calculated for Tm^{3+} ion [11]. The parameters of fourth order are for all our sets about ten times greater and for the sixth order about 50 times greater than PCM values (table 1, last row) giving $\Delta_1 \simeq 0.02$ K. Also some changes occur in the sign of V_4^m and V_6^m which seems to demonstrate the breakdown of simple PCM calculations in $TmCu_2$. This is not surprising, because similar differences in signs and magnitudes compared with PCM values seem to be essential in many other metals where the R ion is placed as an impurity, e.g. Mg, Sc, Lu, Y [12], and for many inter-metallic compounds, e.g. RAl_2 [13].

The origin of these effects is a result of the general crystal potential acting on 4f electrons of the rare-earth ion. This potential may significantly differ from the Coulomb potential owing to the conduction electron screening [14]. We can demonstrate the role

of screening effects in the case of $TmCu_2$ assuming a very simple modification of the PCM. When suggesting that the conduction electrons have s and d character, the former are responsible for the screening of Cu ions while the latter screen the Tm sublattice. The resulting electric potentials from the Cu sublattice and Tm sublattice acting on the localised 4f electron may be considerably different. The Tm and Cu ions were regarded in the usual PCM as ions with charge $+3e$ and $+e$, respectively [5].

Following the discussion above, we treated the ion charge as an effective parameter reflecting the real screening through conduction electrons. The simplest approximation is proposed in which the Cu sublattice is to be fully screened ($Z_{Tm} = 3$ and $Z_{Cu} = 0$). This approach has been demonstrated and discussed in the case of RAl_2, $SmCo_5$ and $SmCo_{17}$ compounds [13, 15, 16]. Moreover the conduction electrons may exhibit a considerable anti-shielding contribution [17] owing to depletion charge arising from an orthogonality hole [18]. Using the usual formulae, the same crystallographic parameters as in [5], the relativistic values $\langle r^l \rangle$ [19] and $\sigma_2 = 0.75$, our simple modified PCM (table 1, penultimate row) requires the anti-shielding parameter δ_6 [17], which must be in this case about 10 in order to obtain $\Delta_1 \simeq 1$ K and $\Delta_{12} \simeq 200$ K.

The influence of conduction electrons on the properties of $TmCu_2$ can be demonstrated also on the negative values of γ_i for the low-lying CEF levels, because the PCM predicts positive values only for Grüneisen parameters of individual CEF levels. The negative γ_i-values are due to a quite complicated volume dependence of the CEF parameters. Negative volume thermal expansion was also observed for $DyCu_2$, $TbCu_2$, $ErCu_2$ [20, 21] and TmSb [22] compounds at low temperatures.

All our fitted sets of CEF parameters are in qualitative agreement with the measured susceptibility ($\chi_b > \chi_c > \chi_a$) and with the saturated moment ($\mu_b = (6.8 \pm 0.2)\mu_B$/ion). We achieved very good agreement for χ_α^{-1} ($\alpha = a$, b and c) at high temperatures ($T > 100$ K) for set Nos 4, 5 and 6 of CEF parameters and $\lambda = 0.429 \times 10^6$ mol m^{-3}. The inverse susceptibility in this region is affected mainly through the second-order parameters V_2^0 and V_2^2, which are close to our experimental values $V_2^0 = (-1.3 \pm 0.3) \times 10^{-23}$ J/ion and $V_2^2 = (-1.4 \pm 0.4) \times 10^{-23}$ J/ion.

The measured and calculated inverse susceptibility curves below 100 K are only qualitatively consistent. The susceptibility measurements in this area can be influenced by experimental uncertainty in the orientation of the sample with respect to the applied field and by the quality of our single crystal. On the other hand we have treated the susceptibility only in the molecular-field approximation assuming the ferromagnetic effective exchange interaction ($\lambda > 0$). The calculated χ_b^{-1} exhibits onset of magnetic saturation near 50 K. This clearly shows that the exchange interaction cannot be fully described within the molecular-field model below 100 K.

6. Conclusion

Our study of the CEF in $TmCu_2$ is based on the analysis of specific heat and volume thermal expansion data. The described method takes advantage of the negative magnitude of the CEF contribution to the thermal expansion (see figure 2), which facilitates determination of the individual components to the specific heat. This allowed us to establish the characteristic features of the CEF energy spectrum ($\Delta_1 \simeq 5$ K; $\Delta_2 \simeq 68$ K; $\Delta_{12} \simeq 210$ K) in comparison with other possible tests (magnetisation, susceptibility and magnetic entropy). The Δ_1-value agrees with preliminary results of inelastic neutron spectroscopy [23]. In spite of the described agreement between experimental and calculated data, the final determination of CEF parameters based on macroscopic experiments is

ambiguous in this low-symmetry case. We believe that inelastic neutron spectroscopy can give a definite answer.

Acknowledgments

We would like to thank Dr V Nekvasil for many helpful discussions and Dr M Loewenhaupt and Dozent Dr E Gratz for kind information about the inelastic neutron spectroscopy results prior to publication. Two of the authors (VS and ZS) wish to express their thanks to Professor J J M Franse (Natuurkundig Laboratorium der Universiteit van Amsterdam) for the opportunity to perform the thermal expansion measurements and to Dr B Lebech (Risø National Laboratory) for the neutron diffraction experiment.

References

[1] Barron T H K, Collins J G and White G K 1980 *Adv. Phys.* **29** 609
[2] Smetana Z, Síma V, Bischof J, Svoboda P, Zajac S, Havela L and Andreev A V 1986 *J. Phys. F: Met. Phys.* **16** L201
[3] Luong N H, Franse J J M and Hien T D 1985 *J. Phys. F: Met. Phys.* **15** 1751
[4] Hutchings M T 1964 *Solid State Phys.* **16** 227
[5] Zajac S, Diviš M, Síma V and Smetana Z 1988 *J. Magn. Magn. Mater.* **76–7** 197
[6] Diviš M, Svoboda P, Smetana Z, Nekvasil V and Andreev A V 1989 *Phys. Status Solidi* b **153** K69
[7] Bowden G J, Bunbury D P and McCausland M A H 1971 *J. Phys. C: Solid State Phys.* **4** 1840
[8] Síma V, Smetana Z, Diviš M, Svoboda P, Zajac S, Bischof J, Lebech B and Kayzel F 1988 *J. Physique Coll.* C8 415
[9] Svoboda P, Smetana Z and Andreev A V 1989 *Phys. Status Solidi* a **111** 285
[10] Smetana Z, Síma V and Lebech B 1986 *J. Magn. Magn. Mater.* **59** 145
[11] Erdos P and Kang J H 1972 *Phys. Rev.* B **6** 3393
[12] Hóg J and Touborg P 1975 *Phys. Rev.* B **11** 520
[13] del Moral A 1984 *J. Phys. F: Met. Phys.* **14** 1477
[14] Orlov V G 1986 *J. Magn. Magn. Mater.* **61** 337
[15] Smit H H A, Thiel R C and Buschow K H J 1988 *J. Phys. F: Met. Phys.* **18** 295
[16] Ballou R, Barthem V M T S and Gignoux D 1988 *Physica* B **149** 340
[17] Das K C and Ray D K 1969 *Phys. Rev.* **187** 777
[18] Cohen M L and Heine V 1970 *Solid State Phys.* **24**
[19] Lewis W B 1971 *Proc. 16th Congr. Ampere* ed I Ursu (Bucharest) p 717
[20] Luong N H, Franse J J M and Hien T D 1985 *J. Magn. Magn. Mater.* **50** 153
[21] Franse J J M, Luong N H and Hien T D 1985 *J. Magn. Magn. Mater.* **52** 202
[22] Ott H R and Lüthi B 1977 *Z. Phys.* B **28** 141
[23] Loewenhaupt M and Gratz E 1989 private communication